Sizing of a Raven-class telescope using performance sensitivities

Ryan D. Coder
Georgia Institute of Technology
Marcus J. Holzinger
Georgia Institute of Technology

Abstract

This work details the sizing and selection of components for a Raven-class telescope to be constructed at the Georgia Institute of Technology, and makes four main contributions. The first is the development of a novel performance metric that quantifies the accuracy of initial orbit estimates generated by the Raven. The second is the derivation of a limiting magnitude metric utilized to bound the detection capability of the Raven. The third is the computation of local sensitivity relationships, which identify the variables that have the greatest impact on Raven system performance metrics. The derived sensitivities can be used to assist the designer in evaluating performance tradeoffs and quantify the amount of improvement in system performance per unit cost. Finally, Raven system performance metrics are used to construct several Pareto frontiers for Ravens operating in different optical environments. The most important insight provided by these Pareto frontiers is that Raven-class telescopes located in optically noisy environments, such as Atlanta, should be designed to maximize the accuracy of initial orbit estimates rather than maximizing detection limit performance. These plots also highlight the diminishing return of increasingly large aperture diameters, demonstrating the value of the Raven design paradigm.

1. Research Motivation

In 2001, the Rumsfeld Commission Report concluded that improvements in Space Situational Awareness (SSA) were needed to protect the US and its allies as well as maintain its economic and diplomatic objectives [1]. Joint Publication 3-14, "Space Operations," defines the high level activities of SSA, which includes the characterization and analysis of space objects (SOs) [2]. Space objects typically consist of active and inactive satellites, rocket bodies, and orbital debris [3]. The U.S. Strategic Command (USSTRATCOM) Joint Space Operations Center (JSpOC) operates the Space Surveillance Network (SSN) and currently tracks 22,000 objects with diameters greater than 10 cm [4]. A key element of JSpOC responsibility is determining whether the orbits of SOs might bring them into close proximity, an event known as a "conjunction," and the conditional probability of SO collision [5]. Additionally, NASA Johnson Space Center's (JSC) Orbital Debris Program Office (ODPO) has primary responsibility for tracking members of the SO population below the SSN detection limit [6]. The need for SSA has been demonstrated by the often cited Chinese anti-satellite test in 2007 [7] and the Iridium/Cosmos collision in 2009 [8]. More recent events including the uncertainty of an alleged conjunction between a Russian satellite BLITS and debris from the Chinese anti-satellite test only serve to further illustrate the growing need for persistent SSA [9].

Scheduling limited sensor resources to collect observations of the large SO population is a complex scheduling and resource allocation problem [10]. Due to the centralized planning yet distributed nature of current SSN sensors [11] and the fast time scales involved in making SO observations, [12, 13] decisions concerning follow up observations are best made locally at the sensor location, and globally on time scales that are incompatible with human in-the-loop decision making. In addition, modifying established schedules under dynamically evolving scenarios, inclement weather conditions, and hardware faults is difficult [10]. The large number of SOs, complex scheduling constraints, and short time scales are persistent challenges that can be addressed using autonomy approaches [14].

The heritage of autonomous telescopes can be traced to automated photoelectric telescopes, first appearing in the mid 1960's at the University of Wisconsin. A 0.2 m telescope was instructed via punched paper tape to observe a fixed sequence of stars in order to measure extinction for larger telescopes. In 1983, the first telescope capable of repeating predefined tasks was used to make UBV measurements of stars for an entire night. This 0.25 m telescope continued to operate for 25 years [16]. The era of prolific autonomous telescopes began in the late 1990s. One example of such as system is the Raven program at the Air Force Research Laboratory (AFRL) Directed Energy Directorate's Air Force Maui Optical and Supercomputing (AMOS) site. A Raven-class telescope system is not rigidly defined by a specific combination of hardware. Rather, it is a design paradigm where commercial off-the-shelf (COTS) hardware and software are combined to fulfill the designated mission requirements. Physically, the Raven system is a combination

of several physical components: the telescope and dome, the CCD, control computer, the weather station, and a GPS receiver and timing system. While the Raven program initially started as an R&D effort, in 2001 a Raven located at the Maui Space Surveillance Site became a contributing sensor to the SSN [10]. Using the weather station sensors, it can detect nautical twilight to begin automated boot sequences and detect inclement weather to suspend operation. Additionally, given a set of tasks, it can determine an appropriate observation schedule to satisfy the human-provided objectives [10]. Other research efforts include The Thinking Telescope program at Los Alamos National Laboratories. This program has taken lessons learned from TALON and has combined additional RAPTOR telescopes with unsupervised learning techniques. The architecture consists of a vast database of observational variations from persistent sources coupled with intelligent agents. These agents learn over time to distinguish between actual gamma ray burst (GRB) events and environment noise such as airplane lights and other non-celestial phenomena [17].

Current efforts at the Georgia Institute of Technology seek to establish an "idea to operation" end-to-end SSA research program. A component of this effort is the construction of a Raven-class telescope, to be located in the Georgia Tech observatory. This Raven will be used for the development of SO detection and characterization algorithms, and can also be used to explore novel, proposed autonomy architectures. The new Raven will be a source of publishable data and will also be utilized through a partnership with the School of Physics for education and outreach. When considering the selection of COTS components for a Raven-class telescope, understanding the impact of sky pollution on system performance is critical. In order to complete an optical telescope design space exploration, it is necessary to first establish a complete space to detector photometry model.

Once this physics-based model is developed, it was important to consider how to compare the utility of competing telescope designs. Thus, the first contribution of this work is the development of two novel performance metrics. The first objective is used to quantify the amount of information generated by a single Raven in a single SO observation. The second objective was developed to quantify the upper bound on the limiting magnitude of the Raven system and minimize the dependence of the limiting magnitude on SO and environmental parameters. The third contribution is the computation of local sensitivity relationships necessary to determine which system variables have the greatest impact on performance metrics. These sensitivities are analytical derived, as there are known relationships between these performance metrics and system design variables. Finally, system performance metrics are used to construct several Pareto frontiers for Ravens operating in different optical environments. These plots afford the analyst an easy to use visualization of the underlying physics, enabling rapid identification of key performance tradeoffs.

2. Methodology

While there are many design parameters when considering the construction of the telescope, the ones that are more easily controlled in the COTS component Raven design paradigm are those listed in Table 1. Thus, these are treated as the independent variables, $\mathbf{x}$, for the purpose of the paper, while all other parameters, $\mathbf{p}$, are fixed at the values shown in Table 2. Several simplifying assumptions are utilized in the radiometric model developed to reduce the complexity of the problem. The first is that the SO are modeled as spheres, and that the specular and diffuse components of reflectivity contribute equally to their signature. Another is that circular orbits are assumed when determining the velocity of SO from orbital altitudes. Also, the number of pixels occupied by a SO on the focal plane is assumed continuous. While all real CCD sensors have discrete pixels, each case is evaluated and the continuous case is found to fully capture the physics of the problem.

2.1 Derivation of Information Objective

SSA telescopes have two goals: to accurately generate initial orbit estimates and to detect the dimmest SOs possible. Because this is an observation task, attempting to estimate arbitrary parameters a from arbitrary discrete data y, the problem can be described using the Fisher Information Matrix, commonly defined as [18]

$$\mathbf{I}(\mathbf{a}) = \int d\mathbf{y} \frac{\partial \ln P_r}{\partial \mathbf{a}} \tag{1}$$

where the probability P_r is equivalent to the likelihood function. Furthermore, the relationship between the Cramer-Rao bounds and the Fisher Information is given by

$$e^2_{\text{min}} = \mathbf{I}(\mathbf{a})^{-1} \tag{2}$$

In a Raven system, the uncertainty in an initial orbit estimate is a combination of uncertainties in the measurement as well as uncertainties in the geometry and dynamics of the SO. This work quantifies the measurement uncertainty by relating the information of each image and the observation noise covariance of an estimation filter, such as a batch estimation filter. In such a filter, a measurement z is made at time k of the true state x as given by Eq. 3 where v is the observation noise which is assumed to be zero mean Gaussian white noise described by Eq. 4 [19].

$$\mathbf{z}_k = \mathbf{h}\left(\mathbf{x}_k\right) + \mathbf{v}_k \tag{3}$$

$$\mathbf{v}_k \sim N\left(0, \mathbf{R}_k\right) \tag{4}$$

Therefore, the relationship between the Fisher Information contained in a single observation and the observation noise covariance is shown by Eq. 5.

$$\mathbf{I} = \mathbf{R}^{-1} = \begin{bmatrix} \sigma_x & 0 \\ 0 & \sigma_y \end{bmatrix} \tag{5}$$

Most COTS CCD detectors utilize square pixels, therefore $\sigma = \sigma_x = \sigma_y$ and Eq. 5 reduces to

$$\mathbf{I} = \mathbf{R}^{-1} = \left(\sigma^2 \mathbb{I}\right)^{-1} = \frac{\mathbb{I}}{\sigma^2} \tag{6}$$

This vectorized result does not yield a single scalar Fischer information quantity, so the volume of the Fisher Information Matrix is computed using the trace operation to obtain the total information [18].

$$\text{tr}(\mathbf{I}) = \frac{2}{\sigma^2} \tag{7}$$

Because the IFOV practically defines the resolution of images captures by the Raven system, it approximately scales with the observation noise covariance. The equation for IFOV, using the small angle approximation, is given by Eq. 8 [20].

$$\sigma \sim \text{IFOV} = 2\arctan\left(\frac{p}{N \cdot D}\right) \simeq 2\left(\frac{p}{N \cdot D}\right) \tag{8}$$

This simplified expression for IFOV is substituted into Eq. 7 above yielding the final expression for the information objective given by Eq. 9.

$$J_I = \ln\left[\frac{(N \cdot D)^2}{p^2}\right] \tag{9}$$

2.2 Derivation of Limiting Magnitude Objective

With the accuracy observations enabling initial orbit determinations defined, the next performance metric to consider is the detection capability of the Raven system. The ability to quantify the upper bound of the total system's SO detection limit is desired. It is also advantageous to decouple this performance metric from noise variables not under the designers control, such as SO and environmental parameters. The arrival process of photons incident on the CCD plane can be accurately modeled by a Poisson process. Schildknecht derives the following relationship for the SNR, by assuming a mean background noise can be determined from z, "SO-free" pixels. [12]

$$\text{SNR} = \frac{S_{so} \cdot t_{\text{int}}}{\sqrt{S_{so} \cdot t_{\text{int}} + m \cdot \alpha\left(S_{\text{sky}} + S_{\text{dark}}\right) t_{\text{int}} + \frac{S_{\text{read}}}{n^2}}} \tag{10}$$

In the SNR equation, $\alpha = 1 + 1/z$, and m is the number of pixels occupied by the SO. For a moving point source, the number of pixels occupied by the incoming signal grows as defined by Eq. 11 where v is in radians/second and IFOV is in radians. [12] It is important to note that v is the relative velocity between the telescope motion and the SO. In this work, the telescope was assumed to be operating only in stare mode, thus the relative v was simply the velocity of the SO [6].

$$m = \begin{cases} m_0 & : v = 0 \\ m_0 + \frac{\sqrt{m_0} \cdot v \cdot t}{\text{IFOV}} & : v \neq 0 \end{cases} \tag{11}$$

To determine the number of pixels initially occupied by the SO, m_0, the effect of seeing needs to be accounted for. In order to preserve the computational efficiency of the code, while still retaining the correct physical trends, the Eq. 12

was utilized. Here, the left hand term defines the number of pixels purely from geometry, while the right hand term is a first order approximation of an Airy disk and its interaction with IFOV. This approximation accounts for the effect of seeing, which is measured in arc seconds as defined by the full width at half maximum.

$$m_0 = \left(\frac{D_{\text{SO}}}{R \cdot \text{IFOV}} + \frac{\text{FWHM}}{206265 \cdot \text{IFOV}} \right)^2 \tag{12}$$

To measure the total system capability, the limiting magnitude objective was set equal to the limit of the SNR equation as the integration time, t_{int}, approaches infinity. However, it is important to note that this capability may not be physically realizable for every SO observation. While both theory and existing telescope programs have shown that this limit is quickly approached in as little time as it takes an SO to cross a few pixels in the image plane, one cannot say a priori that this will always be the case. [12] In order to further make validate this point, an equation was also developed for the time to detect an SO, and it was demonstrated that the limiting magnitude is quickly approached in as little as 10 s of integration time.

Plugging Eq. 11 into the SNR equation while assuming z, and hence α, equal to unity leads to an expanded form of the SNR equation given in Eq. 13. This assumption implies that the frame captured by the CCD has a large, empty background, and thus would not be characteristic of a crowded star field. In Atlanta, this assumption is appropriate but may lead to exaggerated values of limiting magnitude for traditional telescope locations with darker skies.

$$\text{SNR}^2 = \frac{(S_{so} \cdot t)^2}{S_r + \left[S_{so} + m_0 \left(S_{\text{sky}} + S_{\text{dark}}\right)\right] t + \sqrt{m_0} \cdot v \cdot N \cdot D \left(S_{\text{sky}} + S_{\text{dark}}\right) \frac{1}{2p} t^2} \tag{13}$$

Using L'Hospital's rule twice to find the SNR as time grows to infinity determines that maximum achievable SNR, resulting in Eq. 16. The first derivative of Eq. 13 results in

$$\text{SNR}^2 = \frac{2 \cdot S_{so}^2 \cdot t}{\left[S_{so} + m_0 \left(S_{\text{sky}} + S_{\text{dark}}\right)\right] + \sqrt{m_0} \cdot v \cdot N \cdot D \left(S_{\text{sky}} + S_{\text{dark}}\right) \frac{1}{p} t} \tag{14}$$

While the second derivative of Eq. 13 simplifies to

$$\text{SNR}^2 = \frac{2 \cdot S_{so}^2}{\sqrt{m_0} \cdot v \cdot N \cdot D \left(S_{\text{sky}} + S_{\text{dark}}\right) \frac{1}{p}} \tag{15}$$

Simple algebraic manipulation of Eq. 15 produces

$$\text{SNR}_{\text{lim}} = \text{SNR} \lim_{t \to \infty} \simeq \frac{\sqrt{2} \cdot S_{so}}{\left[\sqrt{m_0} \cdot v \cdot N \cdot D \left(S_{\text{sky}} + S_{\text{dark}}\right) \frac{1}{p}\right]^{1/2}} \tag{16}$$

Substituting in for the number of photons emanating from the source, S_{so}, yields

$$E_{\text{SO}} = \frac{\text{SNR}_{\text{lim}} \left[\sqrt{m_0} \cdot v \cdot N \cdot D \left(S_{\text{sky}} + S_{\text{dark}}\right) \frac{1}{p}\right]^{1/2}}{\sqrt{2} \cdot \tau_{atm} \cdot \tau_{opt} \left(\frac{\pi D^2}{4}\right) \cdot QE} \tag{17}$$

The conversion from flux to apparent visual magnitudes is applied, and using a simple law of logarithms results in the final limiting magnitude objective utilized in this study.

$$J_m = 2.5 \log_{10} \left[\frac{\sqrt{2} \cdot E_0 \cdot \tau_{atm} \cdot \tau_{opt} \left(\frac{\pi D^2}{4}\right) \cdot \text{QE}}{\text{SNR}_{\text{alg}} \left[\sqrt{m_0} \cdot v \cdot N \cdot D \left(\dot{S}_{sky} + \dot{S}_{dark}\right) \frac{1}{p}\right]^{1/2}} \right] \tag{18}$$

2.3 Multi-Objective Optimization

In multi-objective optimization, the solutions are always compromise solutions, in that an decrease in the value of one objective can only be gained at the increase of another. The solutions we seek are termed Pareto optimal solutions, and

Table 1: Raven Design Variables

Design Variable	Symbol	Units	Minimum Value	Maximum Value
Aperture Diameter	D	m	.001	.5
F-Number	N	-	1	12
Pixel Size	p	m	$5 \cdot 10^{-6}$	$9 \cdot 10^{-6}$

Table 2: Raven System Parameters

Parameter	Symbol	Units	Value in ATL	Value in Antarctic
SO Altitude	a_{SO}	km	300	300
SO Diameter	D_{SO}	m	1	1
SO Elevation	θ_{SO}	deg	30	30
Irradiance of Magnitude 0 Source	E_0	photons/second/m^2	$5.6 \cdot 10^{10}$	$5.6 \cdot 10^{10}$
Atmospheric Seeing	FWHM	arcsecond	4	1.5
Sky Brightness	M_b	magnitude/arcsecond^2	15	22
CCD Quantum Efficiency	QE	-	.6	.6
CCD Dark Current	S_{dark}	e/pixel/second	.5	.5
SNR Required for Algorithm Detection	SNR_{alg}	-	4	4
Atmospheric Transmittance	τ_{atm}	-	.5	.7
Optical Transmittance	τ_{opt}	-	.9	.9
Secondary Transmittance	τ_s	-	.84	.84

are often depicted as a Pareto frontier, as shown in Fig. 1 A design point $\mathbf{x}$ in the feasible design space is called Pareto optimal if there is no other point $\mathbf{x}$ in the set that reduces at least one objective function without increasing another one. Thus, the ordering of these Pareto points is often referred to as "Pareto dominance." A point may be strongly or weakly dominant, where in a minimization problem a vector of objectives J strongly dominates another vector of objectives $\hat{J}$ if $J < \hat{J}$ and weakly dominates it if $J \leqslant \hat{J}$. Thus, a Pareto frontier is set of strongly non-dominated points in objective space. A scalar value, $\beta = \{0, 1\}$, is used to generate the Pareto dominant designs between the two extreme Pareto points, where performance in one objective is maximum. The two performance metrics are combined into the multi-objective optimization problem shown in Eq. 19. When $\beta = 0$ the design point is optimized for maximum information content, and when $\beta = 1$, the design is optimized for the greatest limiting magnitude. This study took this a step further, and generates a Pareto frontier for each increment of telescope aperture, thus creating a Pareto surface. Additionally, in order to ensure the resulting solutions are not skewed by the order of magnitude difference between the two performance metrics, each is normalized as shown in Eq. 20 [21]. In this equation, the ith objective is evaluated using the current vectors of design variables and parameters. The term ${f_i}^{\circ}$ denotes the utopia point, which is a physically unrealizable solution plotted in the objective space using a vector of each minimum J_i. Conversely, ${f_i}^{\text{max}}$ is the maximum value for J_i.

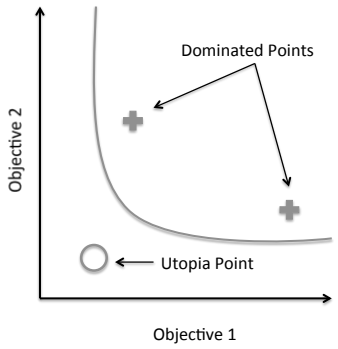

Figure 1: Sample Pareto Frontier

Table 3: Information Content Sensitivities for Raven

Variables	Sensitivity of Information Content	Variable Step Change
Pixel Size	-4	per 1 μm
Aperture Diameter	.4	per .1 m
f-Number	.25	per 1

$$\begin{aligned} \underset{x}{\text{minimize}} \quad & J(\mathbf{x};\mathbf{p}) = -\left[(1-\beta)\, {J_I}^{\text{norm}}(\mathbf{x};\mathbf{p}) + (\beta)\, {J_m}^{\text{norm}}(\mathbf{x};\mathbf{p})\right] \\ \text{subject to} \quad & .001 \leqslant D \leqslant .5 \\ & 1 \leqslant N \leqslant 12 \\ & 5e-6 \leqslant p \leqslant 9e-6 \end{aligned} \tag{19}$$

The selection of an optimization scheme is carefully considered to solve the multi-objective optimization problem given by Eq. 19. Evolutionary algorithms are avoided, as the ability to support selected designs is preferred. Additionally, because the objective functions are analytically derived, it is known that the objective space is continuous and convex. Therefore, the Raven design space is explored via direct computation. It is important to note that while maximization of both indices is the correct objective, the problem has been cast as a classical minimization problem by multiplying the utility function by -1.

$${f_i}^{\text{norm}} = \frac{f_i(\mathbf{x},\mathbf{p}) - {f_i}^{\circ}}{{f_i}^{\text{max}} - {f_i}^{\circ}} \tag{20}$$

3. Results

The methodology outlined previously is utilized to evaluate the performance of a Raven-class telescope in two very different operating environments, as outlined in Table 2. The first location is the Antarctic. Chosen for its dark skies and benign seeing, this site is typical of a traditional observatory location. The second environment is the Georgia Tech observatory, located in Midtown Atlanta, at approximately N $33^\circ\ 46'\ 39''$, W $84^\circ\ 23'\ 55''$. This location exhibits bright skyglow and significant seeing effects which greatly impact the performance of a Raven-class telescope.

3.1 Raven in Antarctica

Fig. 2(a) shows the Pareto surface for a Raven-class telescope located in the Antarctic. The surface shows great curvature, as a result of a decrease in limiting magnitude as the aperture diameter decreases. The convexity of the surface itself can also be seen as the tradeoff is made between information content and limiting magnitude. The solid black line is the line created by the Utopia point for each aperture diameter. Fig. 2(b) shows the Pareto surface looking down the aperture diameter axis, with aperture diameter now shaded as the contour. This plot again highlights the tradeoff made between information and limiting magnitude, for example, as one follows the isoline of constant diameter from the top of the plot towards the bottom. Fig. 2(c) utilizes the information for the shading of the contour as in Fig. 2(a), but this view looks down the limiting magnitude axis. This plot showcases the effect of utilizing long f-numbers and short pixel sizes when maximizing information, as a much greater diameter is needed to achieve the same limiting magnitude. Finally, Fig.2(d) shows the limiting magnitude dependence on aperture diameter if one were to maximize this parameter alone. In this way, the analyst can easily determine if any Raven-class telescope design could meet the design constraints.

If no design were to satisfy the desired performance, or if simply the analyst were looking for ways to incrementally increase system performance, the analytical Jacobians of the performance metrics are utilized to determine which design variables and parameters have the greatest impact on system performance. It is extremely important to note that the sensitives may depend on other variables. Thus changing the value of one variable, may ultimately change the sensitivity of another. Thus, it will be noted that the sensitivities presented here were evaluated using the parameters set forth in 2 and the design variables were fixed to such that the design point was $[D, N, p] = [.5,\ 8,\ 5e^{-6}]$.

Table 3 shows the sensitivities for a Raven telescope in both the Antarctic and Atlanta. These results are valid for

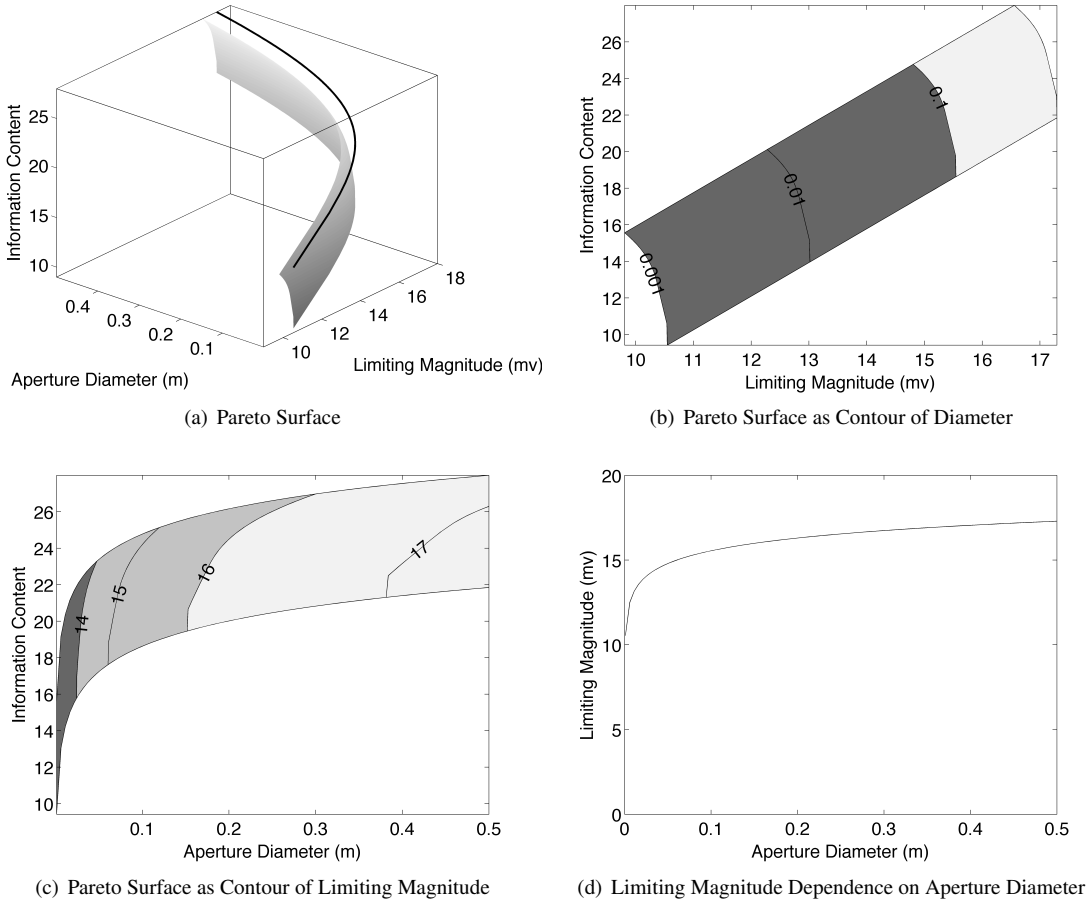

(a) Pareto Surface

(b) Pareto Surface as Contour of Diameter

(c) Pareto Surface as Contour of Limiting Magnitude

(d) Limiting Magnitude Dependence on Aperture Diameter

Figure 2: Raven in Antarctica Continuous Pixels

both locations, as the partial derivatives of the information objective are a function solely of the design variable in question. One can see that the pixel size dominates the effects of either the aperture diameter or the pixel size on the information objective. Also, the aperture diameter affects the information because the performance metrics are developed in terms of f-number rather than focal length. Table 4 lists the sensitivities of limiting magnitude for a Raven in the Antarctic. These sensitivities are not provided in base units, but rather have been converted to increments that would most likely be used by the analyst. Of the three design parameters controllable by the designer, the pixel size has the greatest impact on the limiting magnitude for the conditions and telescope design specified. The SNR required by the detection algorithm is a key driver of the limiting magnitude realizable by the Raven system.

3.2 Raven in Atlanta

Fig. 3 displays the performance of the exact same system located in Midtown Atlanta. Careful inspection reveals a dramatic change in the results, due to the prevalence of light pollution. Examining Fig. 3(a) and 3(b) reveals that there is much less convexity in the Pareto surface. Because the background sky brightness was evaluated with 7 magnitudes difference, the tradeoff between information content and limiting magnitude has become very costly. In fact, Fig. 3(a) reveals that the Utopia line lies very nearly on the top of the surface which optimizes exclusively for information content. This trend is reflected in the nearly vertical isolines of constant limiting magnitude in Fig. 3(c), especially when compared to Fig. 2(c). Lastly, Fig. 2(d) shows that the limiting magnitude of Atlanta compared to the Antarctic is much less, as expected. However, it is interesting to note that in both cases there is 1 magnitude gained between a .1 m aperture diameter and a .5 m aperture diameter. This is especially significant given that aperture diameter is a major driver in the overall cost of a Raven-class telescope. Table 5 lists the sensitivities for the limiting magnitude for a Raven-class telescope in Atlanta. Unsurprisingly, the sky brightness becomes a greater detriment to

Table 4: Limiting Magnitude Sensitivities for Raven in Antarctic

Variable	Sensitivity	Variable Step Change
Pixel Size	7.92E-01	per 1 μm
SO Diameter	-5.41E-01	per 1 m
Sky Brightness	3.18E-01	per 1 mag/arcsec^2
SNR Required for Algorithm Detection	-2.71E-01	per 1
Aperture Diameter	2.17E-01	per .1 m
Atmospheric Transmittance	1.55E-01	per .1
CCD Quantum Efficiency	1.23E-01	per .1
Optical Transmittance	8.23E-02	per .1
CCD Dark Current	-6.60E-02	per .1 e/pixel/second
f-number	-4.98E-02	per 1
Secondary Transmittance	-4.11E-02	per .1
Seeing	-1.57E-03	per 1 arcsec
Orbital Velocity	-9.98E-05	per 1 arcsec/sec
SO Slant Range	9.01E-07	per 1 km
Irradiance of 0 Magnitude Source	1.32E-11	per 1 photon/sec/m^2

the overall detection capability of the system. Also, the design variable of greatest importance to the designer trying to maximize the detection capability for a Raven in Atlanta is the aperture diameter, rather than the pixel size. Also, the required SNR threshold needed by the algorithm again plays a large role in the overall limiting magnitude, as it did in the Antarctic case. This supports the overall goal of assembling a Raven-class telescope at the Georgia Institute of Technology, to serve as a testbed for novel algorithms that could enhance the current state-of-the-art in detection and characterization abilities.

Table 5: Limiting Magnitude Sensitivities for Raven in Atlanta

Variable	Sensitivity	Unit Step Change
SO Diameter	-5.37E-01	per 1 m
Sky Brightness	5.00E-01	per 1 mag/arcsec^2
SNR Required for Algorithm Detection	-2.71E-01	per 1
Aperture Diameter	2.17E-01	per .1 m
Atmospheric Transmittance	2.17E-01	per .1
CCD Quantum Efficiency	9.06E-02	per .1
Secondary Transmittance	-6.46E-02	per .1
Optical Transmittance	6.04E-02	per .1
Pixel Size	1.97E-03	per 1 μm
Seeing	-1.56E-03	per 1 arcsec
fnumber	-6.51E-04	per 1
CCD Dark Current	-1.64E-04	per .1 e/pixel/second
Orbital Velocity	-9.98E-05	per 1 arcsec/sec
SO Slant Range	8.94E-07	per 1 km
Irradiance of 0 Magnitude Source	9.72E-12	per 1 photon/sec/m^2

4. Conclusion

A radiometric model derived from first principles was utilize to investigate the design space for autonomous telescopes. Two novel performance metrics were derived which bound the total detection capability and quantify the ability of the Raven system to make accurate initial orbit estimates. These performance metrics were used as a part of a multi-objective optimization problem, which explored the Raven design space in two optically different operating environments. The results are consistent with intuition, and build confidence that the assumptions made in the radiometric model were sufficient to capture the performance of the Raven system. Sensitivities of the performance

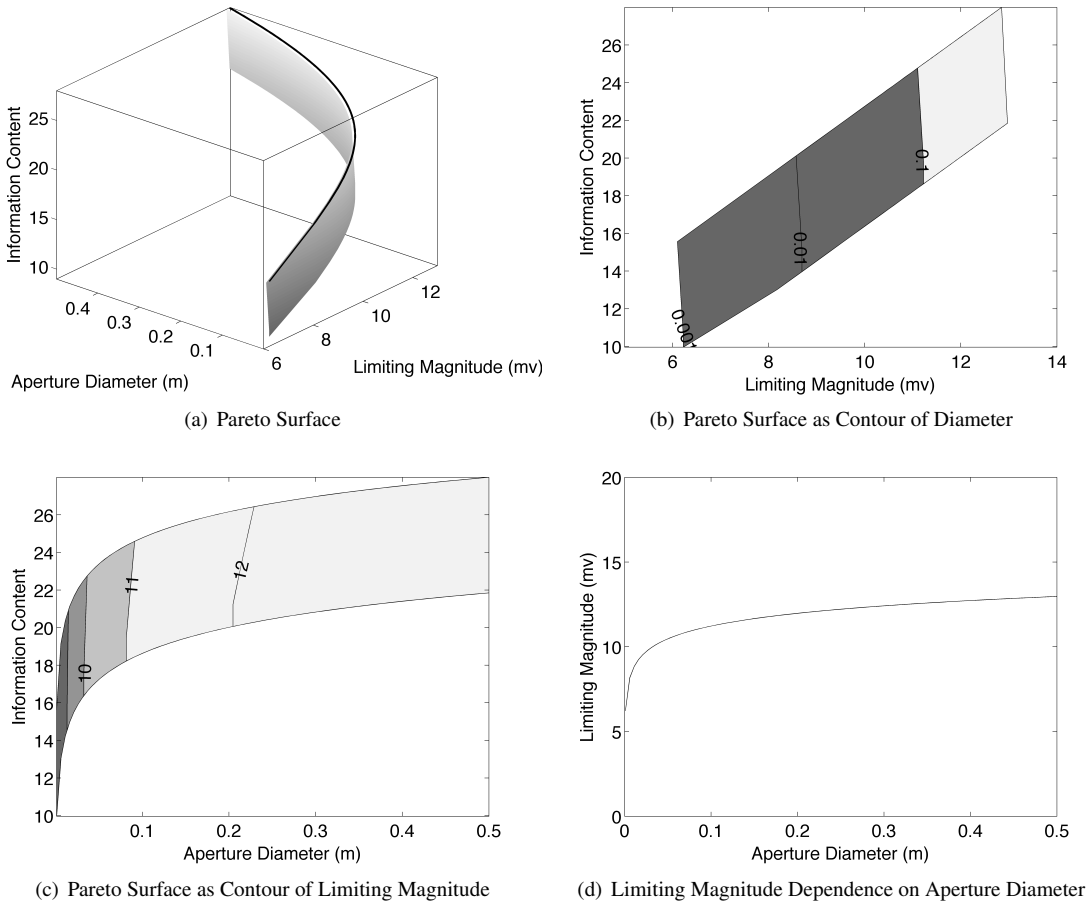

(a) Pareto Surface

(b) Pareto Surface as Contour of Diameter

(c) Pareto Surface as Contour of Limiting Magnitude

(d) Limiting Magnitude Dependence on Aperture Diameter

Figure 3: Raven in Atlanta Continuous Pixels

metrics were also derived, allowing the identification of the major drivers of system performance which may be under the designers control. The impact of the light polluted skies above Atlanta were evaluated. It was found that the bright background skies push the system design towards large f-numbers and small pixel sizes to maximize the information content, and hence accuracy of initial orbit estimates. Also, the difficulty in achieving high limiting magnitudes pushes the aperture diameter as high as the constraint imposed by system cost allows. It was also shown that for both traditional observatory locations and optically noisy environments like Atlanta, the SNR threshold required by the detection algorithm largely influences the overall detection capability of the system. This supports the construction of a Raven-class telescope here in Atlanta to serve as a testbed for novel detection and characterization algorithms. Finally, the diminishing returns of larger aperture diameters demonstrate the efficacy of the Raven design paradigm. It also serves as motivation for future work investigating the capabilities of a distributed sensor network of Ravens with small diameters. It is also noted that future work could involve the investigation of total information rate gain, rather than simply the information capture in a single observation.

References

[1] Donald H. Rumsfeld. Commission to assess united states national security space management and organization. Technical report, Committee on Armed Services of the U.S. House of Representatives, January 2001.

[2] Joint Chiefs of Staff. Space operations. Technical Report JP 3-14, January 2009.

[3] G.H. Stokes, C. Von Braun, R. Sridharan, D. Harrison, and J. Sharma. The space-based visible program. *Lincoln Laboratory Journal*, 11(2):205–238, 1998.

[4] *The Space Report*. Space Foundation, Colorado Springs, CO, 2011.

[5] P. D. Nielsen, K. T. Alfriend, M. J. Bloomfield, J. T. Emmert, Y. Guo, T. D. Maclay, J. G Miller, R. F. Morris, A. B. Poore, R. P. Russell, D. G. Saari, D. J. Scheeres, W. P. Schonberg, and R. Sridharan. Continuing Kepler's Quest: Assessing Air Force Space Command's Astrodynamics Standards. Technical report, National Research Council, Washington, D.C., September 2012.

[6] M. Mulrooney, P. Hickson, E. G. Stansbery, and E. S. Barker. Orbital debris detection and tracking strategies for the nasa/afrl meter class autonomous telescope (mcat). In *61st International Astronautical Congress*, number IAC-10.A6.1.5, Prague, September 2010.

[7] S. Kan. China's Anti-Satellite Weapon Test. Crs report for congress, Congressional Research Service, The Library of Congress, April 2007.

[8] T. S. Kelso. Analysis of the Iridium 33-Cosmos 2251 Collision. In *Advanced Maui Optical and Space Surveillance Technologies Conference*, September 2009.

[9] Amy Butler. No evidence chinese debris damaged russian satellite, 2013.

[10] Chris Sabol, K. Kim Luu, Paul Kervin, Daron Nishimoto, Kris Hamada, and Paul Sydney. Recent developments of the raven small telescope program. *AAS/AIAA Space Flight Mechanics Meeting*, AAS 02-131:397, 2002.

[11] K. Hill, P. Sydney, K. Hamada, R. Cortez, K. Luu, M. K. Jah, P. W. Jr. Schumacher, M. Coulman, J. Houchard, and D. Naho'olewa. Covariance-based network tasking of optical sensors. In *Advanced Maui Optical and Space Surveillance Technologies Conference*, Wailea, HI, September 2010.

[12] Thomas Schildknecht. Optical astrometry of fast moving objects using ccd detectors. In *Geodätisch-geophysikalische Arbeiten in der Schweiz*, volume 49, 1994.

[13] James R. Shell. Optimizing orbital debris monitoring with optical telescopes. In *Advanced Maui Optical and Space Surveillance Technologies Conference*. Space Innovation and Development Center, September 2010.

[14] Defense Science Board. The role of autonomy in dod systems. Technical report, U.S. Dept. of Defense, 2012.

[15] Walt Truszkowski, Lou Hallock, Christopher Rouff, Jay Karlin, James Rash, Michael G. Hinchey, and Roy Sterritt. *Autonomous and Autonomic Systems: With Applications to NASA Intelligent Spacecraft Operations and Exploration Systems*. Springer, 2009.

[16] A. J. Castro-Tirado. Robotic Autonomous Observatories: A Historical Perspective. *Advances in Astronomy*, 2010(570489), 2010.

[17] W. T. Vestrand, D. Heath, W. James, P. Wozniak, N. Ben, R.R. White, J. Bloch, E. Fenimore, B. Hogge, M. Jah, and R. Rast. Autonomous Global Sky Surveillance with Real-Time Robotic Follow-up: Night Sky Awareness through Thinking Telescopes Technology. In *Advanced Maui Optical and Space Surveillance Technologies Conference*, 2008.

[18] B Roy Frieden and Robert A Gatenby. *Exploratory data analysis using Fisher information*. Springer, 2007.

[19] Dan Simon. *Optimal state estimation: Kalman, H infinity, and nonlinear approaches*. Wiley, 2006.

[20] John R. Schott. *Remote Sensing: The Image Chain Approach*. Oxford University Press, 1997.

[21] Jasbir Arora. *Introduction to optimum design*. Academic Press, 2004.